© 2021. Published by The Company of Biologists Ltd | Development (2021) 148, dev200059. doi:10.1242/dev.200059

RESEARCH ARTICLE

A 37 kb region upstream of *brachyury* comprising a notochord enhancer is essential for notochord and tail development

Dennis Schifferl[1,2], Manuela Scholze-Wittler[1], Lars Wittler[1], Jesse V. Veenvliet[1,*], Frederic Koch[1,‡] and Bernhard G. Herrmann[1,‡]

ABSTRACT

The node-streak border region comprising notochord progenitor cells (NPCs) at the posterior node and neuro-mesodermal progenitor cells (NMPs) in the adjacent epiblast is the prime organizing center for axial elongation in mouse embryos. The T-box transcription factor brachyury (T) is essential for both formation of the notochord and maintenance of NMPs, and thus is a key regulator of trunk and tail development. The *T* promoter controlling *T* expression in NMPs and nascent mesoderm has been characterized in detail; however, control elements for *T* expression in the notochord have not been identified yet. We have generated a series of deletion alleles by CRISPR/Cas9 genome editing in mESCs, and analyzed their effects in mutant mouse embryos. We identified a 37 kb region upstream of *T* that is essential for notochord function and tailbud outgrowth. Within that region, we discovered a T-binding enhancer required for notochord cell specification and differentiation. Our data reveal a complex regulatory landscape controlling cell type-specific expression and function of *T* in NMP/nascent mesoderm and node/notochord, allowing proper trunk and tail development.

KEY WORDS: Mouse, Embryo, Development, Notochord, Brachyury, Enhancer

INTRODUCTION

The mammalian embryo is generated in three consecutive phases, starting with head formation from the epiblast, continued by trunk development from the primitive streak acting as growth zone for posterior elongation, and finally tail development from the tailbud. The elongation process is driven by progenitor cells in the growth zone that continuously generate descendants added to the growing anterior-posterior axis (reviewed by Wilson et al., 2009; Wymeersch et al., 2021). Neuro-mesodermal progenitors (NMPs) located in the epiblast at the anterior end of the growth zone, termed node-streak border (NSB), give rise to neural and mesodermal tissues, and beneath, notochord progenitors provide descendants to the node and notochord. The node comprises the trunk organizer involved in medio-lateral patterning of nascent mesoderm (Beddington, 1994; Kinder et al., 2001; Wymeersch et al., 2016). The notochord acts as source of signals patterning the neighboring neural tube, paraxial mesoderm and gut (Stemple, 2005).

The T-box transcription factor brachyury (T) is a key regulator for multiple processes driving axis elongation in vertebrates (Gentsch et al., 2013; Herrmann et al., 1990; Martin and Kimelman, 2008; Stott et al., 1993). Homozygous $T^{-/-}$ mutant mouse embryos lack the node and trunk notochord, fail to form paraxial mesoderm in the trunk, and arrest axial elongation (Chesley, 1935; Gluecksohn-Schoenheimer, 1944). Heterozygous ($T^{+/-}$) mouse mutants are viable, but develop short tails of variable length depending on the extent of the tail notochord (Dobrovolskaia-Zavadskaia, 1927; Gluecksohn-Schoenheimer, 1944).

T activity is essential for notochord formation, notochord differentiation and NMP maintenance (Cambray and Wilson, 2002, 2007; Henrique et al., 2015; Koch et al., 2017; Martin and Kimelman, 2010; Tsakiridis and Wilson, 2015; Tzouanacou et al., 2009). In NMPs, T and the signal molecule Wnt3a form a positive-feedback loop essential for axis elongation and mesodermal lineage choice, the latter in antagonism with the pro-neural activity of Sox2 (Garriock et al., 2015; Koch et al., 2017; Martin and Kimelman, 2008, 2012; Turner et al., 2014). As pan-mesodermal lineage control factor T plays an important role in remodeling the epigenome from the progenitor state to a mesodermal identity, and controls mesodermal transcription factors such as Tbx6 and Msgn1, which are essential for paraxial mesoderm differentiation (Chalamalasetty et al., 2014; Hofmann et al., 2004; Koch et al., 2017; Wittler et al., 2007). The formation and maintenance of the node and notochord require a high level of T expression (Pennimpede et al., 2012; Stemple, 2005; Zhu et al., 2016). The dual essential role of T in NMPs and node/notochord demonstrate that T is the central transcription factor coordinating the organization of the progenitors and their descendants shaping the trunk and tail.

The detailed analysis of *T* control in these processes promises deeper insight into the mechanisms controlling the NMP/NSB domain. T expression is maintained in NMPs and in the node and notochord, but is transient in nascent mesoderm due to repression by Tbx6 (Gouti et al., 2017; Koch et al., 2017). The *T*-streak promoter (from −500 bp to the TSS) is sufficient for *T* expression in nascent mesoderm, but not in the notochord (Clements et al., 1996; Perantoni et al., 2005), and responsive to Wnt signaling (Arnold et al., 2000; Yamaguchi et al., 1999). The control elements for node and notochord expression of *T* have not been identified yet.

Here, we have generated a series of *T* deletion alleles in mouse ESCs by CRISPR/Cas9 technology, and present a detailed analysis of mutant embryos. We show that a 37 kb region upstream of *T* is essential for notochord specification and tail bud outgrowth, and

[1]Max Planck Institute for Molecular Genetics, Department of Developmental Genetics, Ihnestr. 63-73, 14195 Berlin, Germany. [2]Institute of Biology, Department of Biology, Chemistry and Pharmacy, Freie Universität Berlin, Königin-Luise-Str. 1-3, 14195 Berlin, Germany.
*Present address: Max Planck Institute of Molecular Cell Biology and Genetics, Stembryogenesis Group, Pfotenhauerstraße 108, 01307 Dresden, Germany.

‡Authors for correspondence (koch@molgen.mpg.de; herrmann@molgen.mpg.de)

F.K., 0000-0002-0142-2411; B.G.H., 0000-0002-2192-8188

Handling Editor: Patrick Tam
Received 28 July 2021; Accepted 8 November 2021

Development (2021) 148, dev200059. doi:10.1242/dev.200059

identify an enhancer that controls *T* expression in the notochord within that region.

RESULTS AND DISCUSSION

The activity of the *T* promoter in NMPs and nascent mesoderm, in combination with the failure of notochord formation in the T^{Bob} mutant (Rennebeck et al., 1995) suggested that regulatory elements controlling *T* expression in the notochord are located far upstream of *T*. In search of such elements, we used CRISPR/Cas9 technology to generate deletion alleles in mESCs comprising the entire *T* region or a 37 kb upstream region (Fig. 1A), and analyzed their effects on embryonic development using the tetraploid complementation assay (Eakin and Hadjantonakis, 2006).

Immunofluorescent staining showed the expected expression of T in the notochord, NMPs and nascent mesoderm of wild-type embryos (Fig. 1B-C″, Wymeersch et al., 2016). A *T* deletion termed T^{CD} spanning from −62 kb upstream to 10 kb downstream of *T*, including the *T* transcription unit, resulted in axial truncation and absence of the trunk notochord in homozygous embryos, as expected from the analysis of the original *T* mutant (Fig. 1D,D′, Chesley, 1935). The axial truncation phenotype is demonstrated by the depletion of NMPs and differentiation of their descendants into neural tissue at the expense of paraxial mesoderm (Koch et al., 2017), as visualized by an expansion of the neural plate identified by Sox2 protein, and lack of (pre-)somitic mesoderm posterior of the forelimb buds (Fig. 1E-E″).

Embryos carrying the 37 kb deletion, from −8.5 kb to −45.5 kb upstream of *T* comprising the T^{Bob} integration site, (T^{UD}/T^{UD}) appeared almost normally developed at the early tailbud stage with fore- and hindlimb buds, somites and tailbud (Fig. 1F). Optical

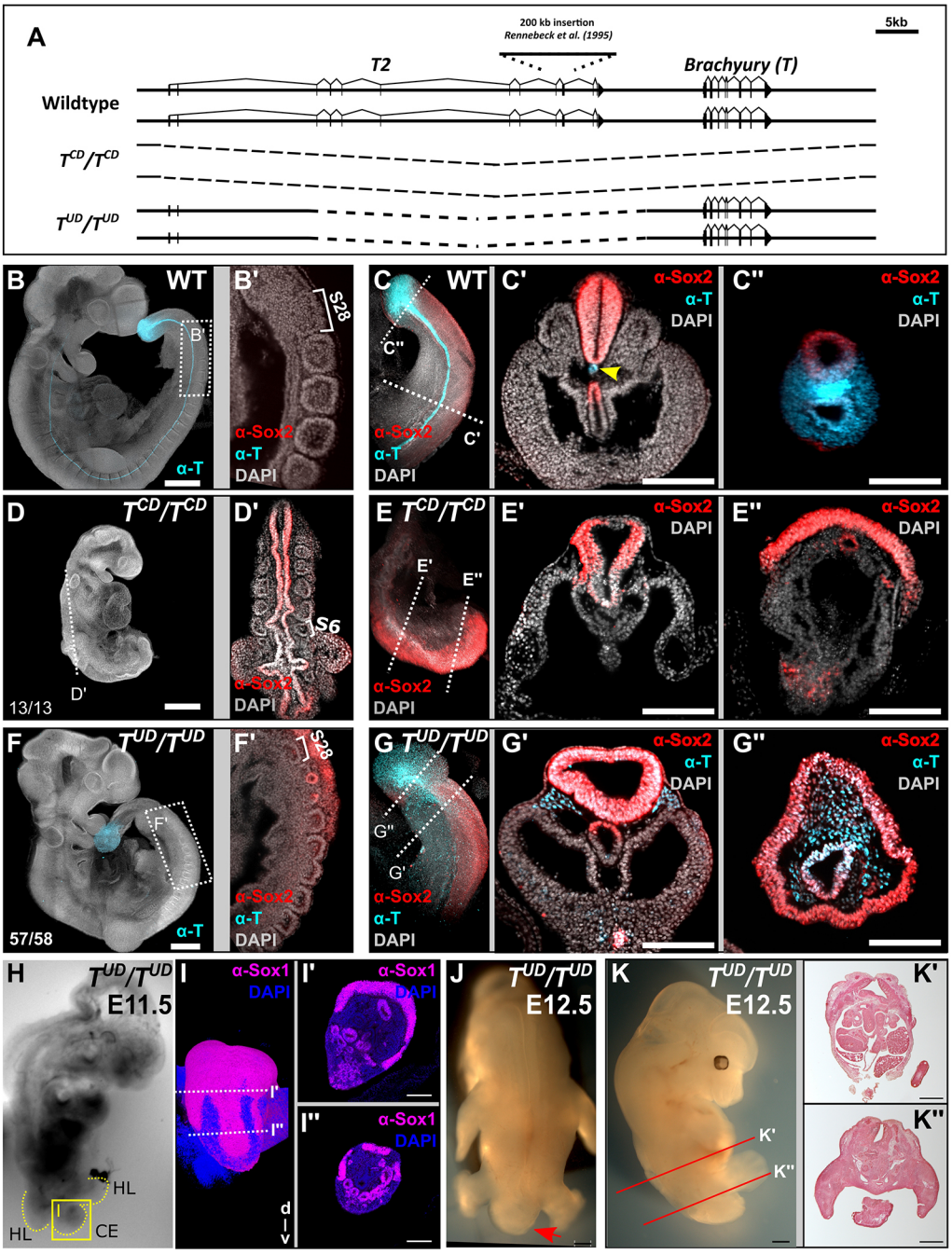

Fig. 1. A 37 kb upstream region contains regulatory elements essential for notochord formation and tailbud outgrowth. (A) Schematic showing the murine *T2-T* locus. (B-G″) Immunostaining for T (cyan) and Sox2 (red) protein with nuclear DAPI (grey) staining in wild type (WT), *T* complete deletion (T^{CD}/T^{CD}) and *T* upstream deletion (T^{UD}/T^{UD}) E9-E9.75 embryos. (B,D,F) Maximum intensity projections of confocal stacks. Scale bars: 500 µm. (B′-C″,D′-E″,F′-G″,I′-I″) Optical sections with light sheet microscopy. Scale bars: 200 µm; number of somites formed is indicated (B′,D′,F′). The yellow arrowhead indicates the notochord (C′). (H) Bright-field image. CE, caudal end; HL, hindlimb. Yellow box marks the domain shown in I. (I-I″) Maximum intensity projection of stacks acquired by light sheet microscopy and single planes. (J) Dorsal view (red arrow indicates caudal end), (K) lateral view and (K′,K″) histological sections; axial levels are as indicated in K. Scale bars: 500 µm.

Development (2021) 148, dev200059. doi:10.1242/dev.200059

sectioning and antibody staining for T and Sox2, however, revealed major defects. Trunk somites appeared smaller than in wild-type embryos and malformed (Fig. 1F′). The notochord was missing in the mutants (Fig. 1F′-G′). In the caudal end and tailbud, paraxial mesoderm was strongly reduced, whereas neural tissue marked by Sox2 protein was largely expanded and surrounding the entire tailbud, which lacked notochordal cells (Fig. 1G′,G″). T expression was detected in cells of the tail gut and was stronger than in adjacent mesoderm. Sox1 staining of E11.5 T^{UD}/T^{UD} embryos showed massive expansion of neural tissue in the caudal end (Fig. 1H-I″, Fig. S1A-F), and histological sections from E12.5 embryos revealed major defects in neural tube and somite differentiation in the trunk (Fig. 1J-K″; Fig. S1G-L). The tail was not formed.

The data show that the 37 kb upstream region contains control elements essential for tailbud formation, tail outgrowth, and proper neural tube and somite differentiation, whereas T expression from the streak promoter is sufficient to support trunk formation from NMPs. The trunk phenotype can be attributed to the lack of signaling inputs from the missing notochord (Chiang et al., 1996). The failure of proper tailbud formation is explained by NMP differentiation towards neural tissue at the expense of mesoderm, accompanied by NMP loss preventing tail outgrowth.

Next, we searched for regulatory elements within the 37 kb region. As T expression in the notochord is maintained for several days, we suspected that T might be controlling its own expression in an autoregulatory manner via a notochord-specific enhancer. To search for T-binding sites in notochord precursors, we generated a *Noto::H2B-mCherry* (Noto^{mC}) reporter construct by BAC recombineering, integrated the modified BAC into ES cells and validated proper reporter expression in transgenic embryos (Fig. S2). We then modified a protocol allowing differentiation of mESCs into Noto-positive cells *in vitro* (Winzi et al., 2011), generated Noto^{mC}+ cells and performed ChIP-Seq using a T antibody (Fig. S3). The ChIP-Seq data identified a strong T peak about 38 kb upstream of the transcriptional start site of T (Fig. 2A). The peak position matches a strong T peak previously identified in NMPs (Koch et al., 2017) and coincides with exon 5 of *T2*. A genomic sequence comparison showed that the region of the peak is conserved in human, chimpanzee, cow and chick, suggesting that it may act as an enhancer (Fig. 2B).

We tested whether the T peak element is able to drive expression of a reporter in transgenic embryos. We cloned a 653 bp genomic fragment comprising the T peak region containing a palindromic T consensus binding site upstream of a HSP68 minimal promoter – Venus reporter (Fig. S4). The fragment also contains two consensus sites for Foxa2, another transcription factor essential for node and notochord formation (Ang and Rossant, 1994; Weinstein et al., 1994). We integrated the reporter construct into a *Rosa26*-close locus engineered for single copy integration using Cre recombinase in ES cells (Vidigal et al., 2010) and assayed mid-gestational embryos by fluorescence microscopy. The data show Venus expression primarily in the node and notochord at E8.5 and E9.75, confirming that the T peak element comprises a notochord enhancer bound by T (Fig. 2C). We therefore designated this element *TNE* (T-bound notochord enhancer).

Next, we genetically modified the T locus in the Noto^{mC} reporter ESC line using CRISPR/Cas9. We deleted *TNE* alone or in combination with a 63 kb genomic fragment spanning the *T* gene and upstream region (T^{LD}) in ESCs (Fig. 3A; Fig. S5). We generated homozygous mutant embryos lacking *TNE* ($T^{\Delta TNE/\Delta TNE}$), and analyzed the effect of *TNE* loss on notochord formation and embryogenesis in comparison with wild-type embryos, embryos heterozygous for T^{LD} ($T^{LD}/+$) or compound heterozygotes carrying *ΔTNE* opposite to T^{LD} ($T^{LD}/T^{\Delta TNE}$) (Fig. 3B-I; Fig. S5). At E9.75, wild-type embryos showed correct expression of the reporter in the node and notochord (Fig. 3B). At E11.5, mCherry expression in wild-type embryos was strongest in the caudal end of the tail notochord (Fig. 3C). E9.75 $T^{LD}/+$ embryos appeared normal, though malformed notochord was observed in the caudal trunk of some specimens (Fig. 3D). In contrast, in some E11.5 $T^{LD}/+$ embryos the tail notochord extended only half way into the tail, and the tailbud contained only very few Noto^{mC}+ cells in the gut and ventral neural tube (Fig. 3E). These data show that notochord formation in $T^{LD}/+$ embryos was supported initially, but disrupted more posteriorly as notochord progenitors were incorrectly specified.

In E9.75 $T^{\Delta TNE}/T^{\Delta TNE}$ embryos, T expression in the trunk notochord appeared weaker than in wild-type or $T^{LD}/+$ embryos, and an irregular trail of Noto^{mC}+ cells lacking T protein extended into the tailbud (Fig. 3F). At E11.5, Noto^{mC}+ cells of the tail region were widely dispersed, mostly in mesoderm, and not confined to the midline (Fig. 3G; Fig. S6). The tailbud contained few dispersed Noto^{mC}+ cells, some in a tubular structure located between the neural tube and gut expressing Sox2 and Foxa2, but no T protein anterior to the tailbud (Fig. 3G; Fig. S6). The notochord was lacking, and tail outgrowth reached about half the normal length in these mutants.

The strongest phenotype was observed in $T^{LD}/T^{\Delta TNE}$ embryos (Fig. 3H,I). A notochord was not detectable in the trunk or in the tail, as demonstrated by T antibody staining. At E9.75, Noto^{mC}+ cells devoid of T protein were detected in patches along the midline of the trunk and early tailbud (Fig. 3H). Noto^{mC}+ cells were not detectable in the outgrowing tail at E11.5, which reached a length of about 10 somites (Fig. 3I). The tailbud was disorganized, splitting into two to three subdomains. A similar tail phenotype has been observed in $Gdf11^{-/-}$ embryos showing almost complete absence of T in the tailbud notochord (Jurberg et al., 2013).

In all genotypes the tail outgrowths of E11.5 embryos showed T expression in the tailbud, and somite formation up to the point where the tailbud appeared malformed and further outgrowth started to fail. Differentiation was impaired in the entire region lacking a proper notochord, resulting in severe malformation of the posterior trunk ($T^{LD}/T^{\Delta TNE}$) and/or degeneration of the tail (all mutants). Noto^{mC}+ cells lacking T protein were not specified as notochord cells and instead contributed to neighboring tissues. $T^{LD}/T^{\Delta TNE}$ embryos generated only a few tail somites and the other mutants did not complete tail formation either. Both $T^{LD}/T^{\Delta TNE}$ and $T^{\Delta TNE}/T^{\Delta TNE}$ mutants developed a tailless phenotype; the tail phenotype of $T^{LD}/+$ embryos varied from short tailed to tailless (Fig. 3J-M). Antibody staining for Casp3 revealed massive apoptosis (Fernandes-Alnemri et al., 1994) in the tailbud and tail somites of E11.5 $T^{\Delta TNE}/T^{\Delta TNE}$ and $T^{LD}/T^{\Delta TNE}$ embryos lacking the notochord, thus providing a plausible explanation for the short-tailed or tailless phenotype (Fig. S7; Teillet et al., 1998).

To rule out the possibility that the $T^{\Delta TNE}/T^{\Delta TNE}$ phenotype was due to the deletion of exon 5 of T2, we generated mutations in both alleles of exon 2, resulting in frame shifts of the predicted open reading frame ending in premature stop codons (Fig. S8). E12.5 embryos derived from mutant $T2^{-/-}$ ES cells showed no defect in tail or in trunk development, confirming that the $T^{\Delta TNE}/T^{\Delta TNE}$ phenotype is not caused by the lack of T2, but due to the missing notochord enhancer.

Development (2021) 148, dev200059. doi:10.1242/dev.200059

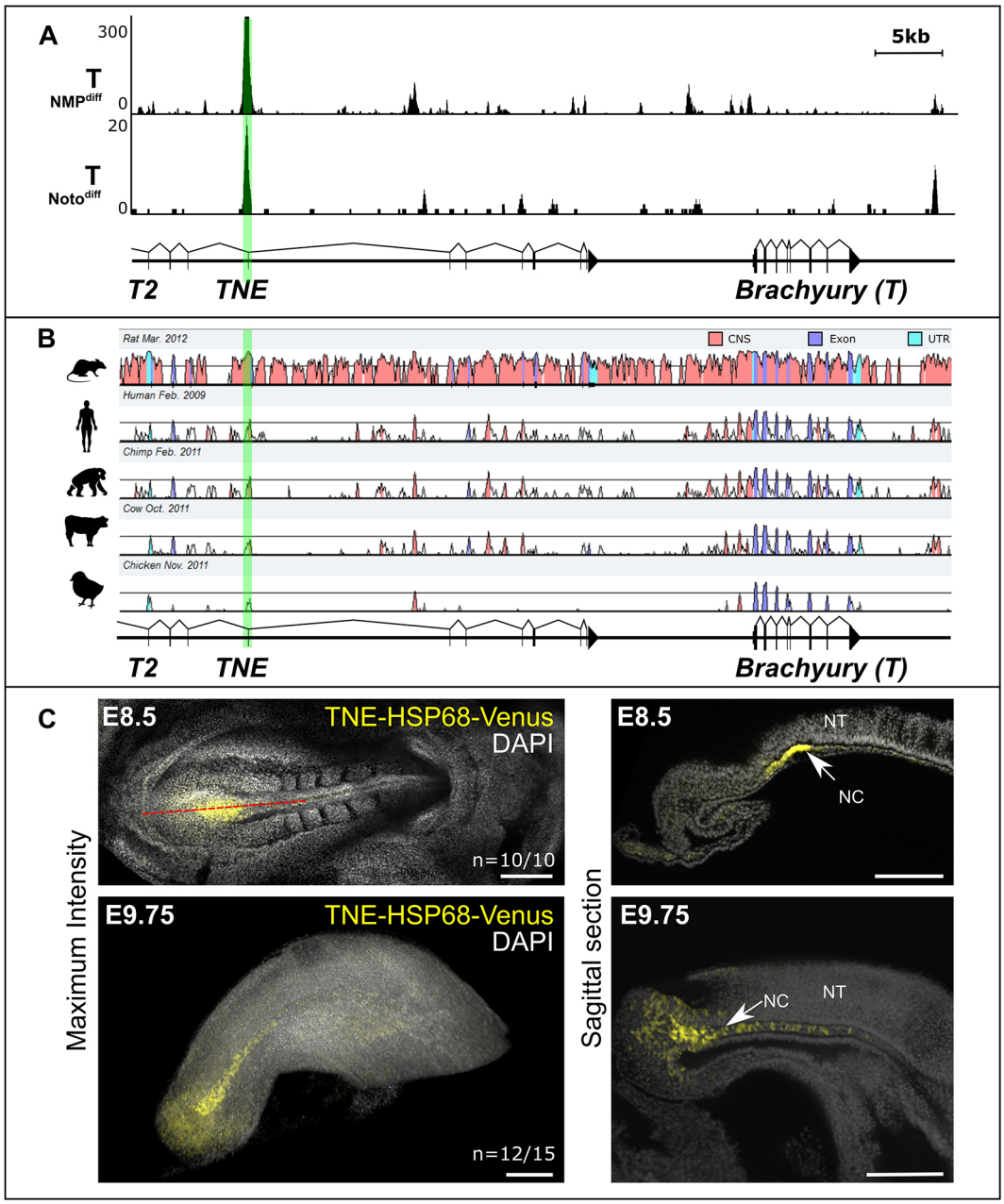

Fig. 2. A conserved T-bound genomic fragment shows enhancer activity in the notochord. (A) ChIP-Seq tracks showing T peaks at the T locus in *in vitro*-derived NMPs (NMP^{diff}; Koch et al., 2017) or notochord-like cells ($Noto^{diff}$). The *TNE* region is highlighted in green. (B) Plot of corresponding genomic sequences in rat, human, chimp, cow and chicken against the mouse T locus (chr17:8,386,974-8,452,208; mm10). CNS, conserved non-coding sequence. (C) *TNE*-driven Venus reporter expression demonstrates enhancer activity in nascent axial mesoderm. Nuclei stained with DAPI (grey). Left: maximum intensity projections of confocal microscopy. Right: sagittal optical sections; light sheet acquisitions. NC, notochord; NT, neural tube. Scale bars: 200 µm.

As formation of the head process notochord does not require T (Wilkinson et al., 1990; Yamanaka et al., 2007), we asked whether the *TNE* or T^{UD} deletion affect notochord differentiation in the head and neck region. We found that the notochord expressing T, Foxa2 and $Noto^{mC}$ had formed in both $T^{\Delta TNE}/T^{\Delta TNE}$ and T^{UD}/T^{UD} mutant embryos at E8.25 (Fig. 4A-C). However, at E9.5 the notochord was missing from this region in T^{UD}/T^{UD} embryos, accompanied by integration of $Noto^{mC}$+ cells into the foregut (Fig. 4D-I). Foxa2 protein was detected in the ventral neural tube, but the Olig2 and Nkx2.2 domains were ventrally shifted, suggesting impaired floor plate maintenance (Fig. 4H,I). Strong ventral neural tube patterning defects were detected in the trunk (Fig. 4J-O). $T^{\Delta TNE}/T^{\Delta TNE}$ mutant embryos were not affected (Fig. 4F,G,L,M). The data suggest that *TNE* is not essential for head process notochord maintenance and differentiation, or for trunk notochord function.

The data show that *TNE* is a functional control element essential for T expression in the notochord, and for notochordal cell specification and differentiation. Reduced T expression in the trunk notochord of $T^{\Delta TNE}/T^{\Delta TNE}$ mutants and absence of T expression and notochord in $T^{LD}/T^{\Delta TNE}$ and T^{UD}/T^{UD} embryos suggest the existence of another notochord enhancer (provisionally termed *NE2*) involved in notochord development, located in the region deleted in T^{UD}. Loss of *TNE* can be compensated for in the head and neck region as well as in the trunk, but not in the tail, by

Development (2021) 148, dev200059. doi:10.1242/dev.200059

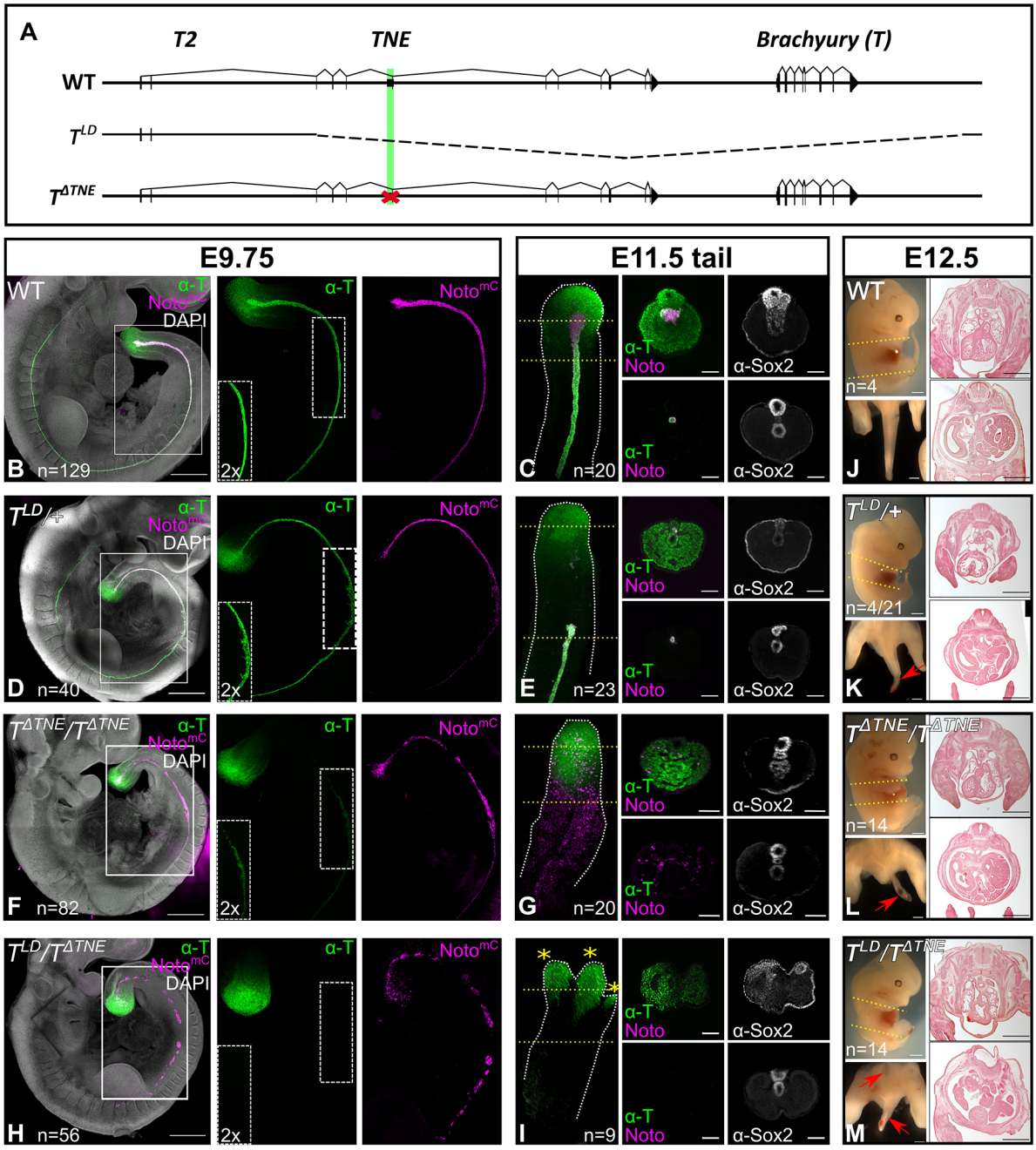

Fig. 3. *TNE* is essential for brachyury expression in NPCs, and for notochord formation and differentiation. (A) Schematic of deletion alleles. (B,D,F,H) Maximum intensity projections of E9.75 embryos with Noto^{mC} reporter signal, immunostaining for T (green) and DAPI nuclear staining (grey). Scale bars: 500 µm. The rectangle indicates the area magnified in single channels. 2× enhanced signal shown in the bottom left panel of the T channel. (C,E,G,I) Maximum intensity projections of E11.5 tails with immunostaining for T (green) and the Noto^{mC} reporter signal (magenta). Asterisks indicate bifurcations of the tailbud; yellow dashed lines indicate the position of optical sections: Scale bars: 100 µm. (J-M) Lateral and top views of E12.5 embryos, and histological transverse sections; section planes are indicated by yellow lines, defects in trunk (M) or tail (K,L,M) are indicated by red arrows. Scale bars: 500 µm. (D,E,K) T^{LD}/+ embryos showed a variable tail phenotype (11/23 had a truncated and 12/23 no tail notochord at E11.5; 17/21 were tailless and 4/21 were short tailed at E12.5); a short-tailed embryo is shown here.

NE2. A single copy of *NE2* in the absence of *TNE*, however, is not sufficient for notochord formation in the trunk or in the tail. Thus, the *T* gene dose and overall expression level in notochord cells are important for the phenotypic outcome. Strikingly, tail notochord formation and differentiation require two wild-type alleles of *T* in cis with *TNE* and possibly also *NE2*. The point where maximal *T* activity is required appears to coincide with the region where notochord progenitors need to expand in order to support proper tail notochord development and tail differentiation, i.e. in the posterior trunk (roughly at the lumbo-sacral transition; Yamanaka et al., 2007, Ukita et al., 2009). The variable tail length of T^{LD}/+ embryos suggests that the genetic background, and thus again the T expression level achieved by individual *T* alleles, can modulate the extension of the tail notochord.

The combined data suggest that the level of T expression in notochord progenitors in the posterior trunk might be related to the

Development (2021) 148, dev200059. doi:10.1242/dev.200059

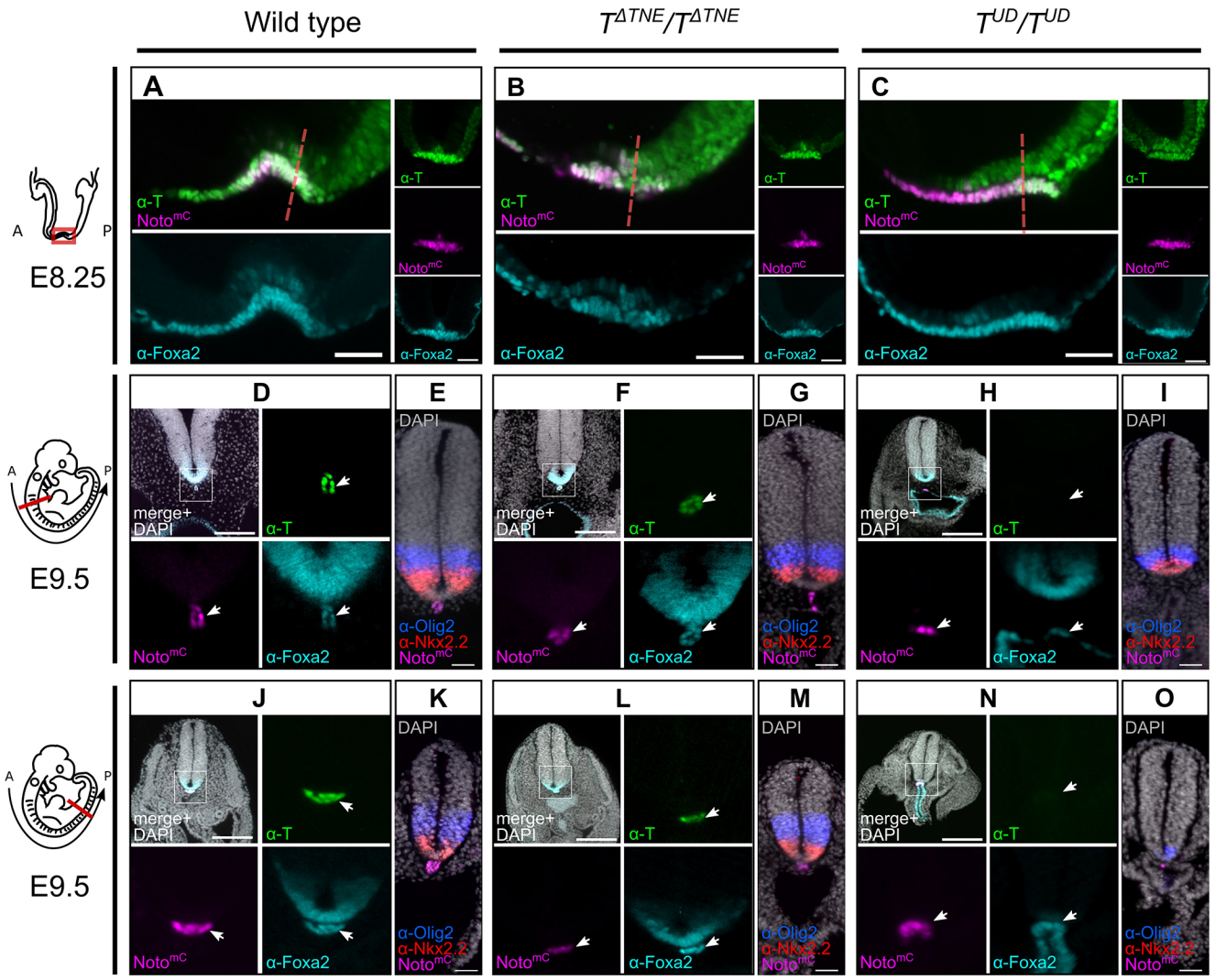

Fig. 4. Head process notochord is formed but not maintained in T^{UD}/T^{UD} mutants. Light sheet micrographs of wild-type and mutant embryos with immunofluorescence for T (green) and Foxa2 (cyan) or Olig2 (blue) and Nkx2.2 (red). (A-C) Sagittal and transversal optical sections of the node at E8.25. Scale bars: 50 µm. (D-O) Transversal optical sections at different axial positions at E9.75, as indicated in the schematic on the left. (D-I) Cervical. (J-O) Lumbar. Scale bars: 200 µm in D,F,H,J,L,N; 50 µm in E,G,I,K,M,O. D,F,H,J,L,N and E,G,I,K,M,O show different embryos.

number of NPCs generated during expansion (Ukita et al., 2009; Wymeersch et al., 2019; Yamanaka et al., 2007), and thus the length of the tail, as tail differentiation is strongly dependent on notochord extension into the outgrowing tail. NMPs need much lower T expression levels than NPCs to function properly, and thus in *T* notochord enhancer mutants initial tail outgrowth can comprise multiple somite pairs. However, tailbud outgrowth beyond the notochord is limited, supporting the view that functional NPCs may form a niche for NMP maintenance (Edri et al., 2019; Wymeersch et al., 2019), although other explanations are conceivable.

MATERIALS AND METHODS

Generation of Noto reporter mESCs

A BAC containing ~200 kb C57/BL6 genome surrounding the mouse *Noto* gene (RP23-289M19) was obtained from BACPAC resources. In order to engineer the Noto::H2B-mCherry reporter, a construct containing a H2B-fused fluorescent mCherry marker was inserted into the start codon of the gene via Red/ET recombineering (Muyrers et al., 1999). The reporter construct is followed by a *FRT*-site flanked selection cassette. The selection cassette consists of a *Pgk* promoter for expression in mESCs and an em7 promoter for selection in bacteria using the hygromycin resistance gene terminated by a *b-globin* polyadenylation signal.

In this study, male mESCs of the G4 hybrid line 129S6/SvEvTac×C57BL/6Ncr (George et al., 2007) served as the parental wild-type clone. All cell lines were regularly tested for possible mycoplasma contamination, using PCR Mycoplasma Test Kit II (Applichem A8994) according to the manufacturer's recommendations.

For random integration of the *Noto::H2B-mCherry* BAC, 5 µg of BAC DNA were linearized using PI-SceI (New England Biolabs R0696S) and electroporated into 3×10^6 wild-type mESCs. Approximately 30 h after electroporation, selection was started applying 150 µg/ml hygromycin B (Merck 10843555001). Selection medium was refreshed daily until single colonies were clearly visible. Single clones were picked and genotyped by PCR. Oligonucleotides used in this study are listed in Table S1.

Generation of deletion alleles

Vectors px335A_hCas9_D10A_G2P (a gift from Boris Greber, Max Planck Institute for Molecular Biomedicine, Münster, Germany) and px459-pSpCas9-2A-Puro (Addgene plasmid #48139) were used for the double nickase or conventional approach, respectively. Both vectors contain sequences encoding the *Streptococcus aureus* Cas9 enzyme controlled by a ubiquitous promoter, the guide RNA controlled by a human U6 promoter,

Development (2021) 148, dev200059. doi:10.1242/dev.200059

a puromycin resistance gene for selection in ESCs and an ampicillin resistance for selection in bacteria. The CRISPR/Cas9 system was used for the introduction of targeted genomic deletions. Close to the desired break points, specific targeting sites 5′-N_{20}*NGG*-3′ were identified and evaluated using the CRISPOR (http://crispor.tefor.net/crispor.py) tool. In cases where the first nucleotide of the N_{20} targeting sequence was not a guanine, a guanine residue was added to the 5′end. For cloning, *BpiI* overhangs, 5′-CACC-3′ or 5′-AAAC-3′ were added to the target sequence or complementary strand sequence, respectively (Table S1).

Transfection of plasmids for CRISPR/Cas9 mediated deletions was performed using Lipofectamine 2000 reagent (Invitrogen 11668027). On the day before transfection, 3×10^5 cells per well were seeded on gelatinized and wild-type feeder coated well of a six-well plate (Corning 3516). After overnight incubation, transfection mixes were prepared. For transfections in a six-well format, mixes of 125 µl Opti-MEM Reduced Serum Medium (Thermo Fisher 31985062) and 8 µg of each vector and 110 µl Opti-MEM and 25 µl Lipofectamine 2000 were prepared. 125 µl of each mix were combined, mixed well and incubated at room temperature for 15 min. Subsequently, 250 µl of transfection complex mix was diluted in 1.25 ml ES+LIF, added to the cells and incubated for 5 h. Finally, cells were trypsinized, split in 3:6, 2:6 and 1:6 ratios, and seeded on 6 cm dishes coated with puromycin resistant mEFs. 24 h post-transfection, transient selection was started applying 3 ml ES+LIF containing 2 µg/ml puromycin (Gibco 10130127) for 2 days and 3 ml ES+LIF containing 1 µg/ml puromycin (Gibco 10130127) for 1 day. After selection, ES+LIF medium was refreshed daily until colonies were clearly visible. Single clones were picked and screened by PCR, and verified by Sanger sequencing of purified PCR products extracted from agarose gels after electrophoresis. In the event that single PCR bands could not be separated by electrophoresis, fragments were cloned into pCR2.1 vectors using the reagents of a TA cloning kit (Invitrogen K202020) according to the manufacturer's procedure.

Generation of enhancer reporter mESC lines

For recombinase-mediated cassette exchange, 3×10^5 mESCs with a modified Rosa26 harboring locus (Vidigal et al., 2010) was co-transfected with 5 µg of linearized TNE-HSP68-Venus construct and 1 µg PGK-iCre vector using Lipofectamine 2000 as described above. For stable selection, cells were cultured in ES+LIF containing 350 µg/ml geneticin (Thermo Fisher 10131027).

Generation of transgenic embryos

Transgenic mouse embryos were generated by diploid or tetraploid morula aggregation by the transgenic unit of the Max Planck Institute for Molecular Genetics in Berlin as described previously (Eakin and Hadjantonakis, 2006). All animal experiments were performed according to local animal welfare laws and approved by local authorities (covered by LaGeSo licenses G0243/18 and G0247/13).

Embryo isolation

Timed pregnant foster mice were euthanized by carbon dioxide application and cervical dislocation. Embryos were isolated from uteri in 4°C pre-cooled PBS. After transfer to glass vials (Wheaton 224882), embryos were fixed in 4% paraformaldehyde (PFA)/PBS (Sigma Aldrich P6148). Fixation times were adapted to embryonic stage and subsequent procedures. For immunofluorescence, E6.5-E8.5 embryos were fixed for 40 min, E9.5-E10.5 for 1 h and E11.5 to E12.5 for 2 h. After fixation, embryos were washed three times with PBS and stored at 4°C until further processing.

Whole-mount immunofluorescence and tissue clearing

If not specified otherwise, incubation in buffers was performed at room temperature on a roller. Embryos selected for immunofluorescence were collected in 4 ml glass vials (Wheaton 224882) and washed doe 3×10 min with PBS and for 3×10 min at room temperature with PBST (PBS containing 0.5% Triton X100, Merck 9002-93-1). For blocking, embryos were incubated in PBSTB (PBST containing 10% FBS) at 4°C for a minimum of 24 h. Primary antibody incubation was performed in PBSTB at 4°C for 48-96 h (antibodies are listed in Table S2). After incubation, remaining antibody solution was diluted by rinsing the samples three times with PBSTB followed by washing for 3×10 min with PBSTB and for 3×10 min in PBST. After washing, the specimens were incubated in PBSTB at 4°C overnight. Secondary antibody incubation was performed in PBSTB at 4°C for 24–48 h. Embryos were rinsed three times in PBSTB and washed for 2×20 min with PBSTB+0.02% DAPI (Roche Diagnostics 102362760019), for 3×20 min PBST+0.02% DAPI and transferred to eight-well glass bottom slides (Ibidi 80827). After additional washing steps in PBS for 3×10 min, embryos were either imaged or processed for tissue clearing.

For tissue clearing, stained embryos on eight-well glass slides were incubated in 0.02 M phosphate buffer (PB, 0.005 M NaH_2PO_4 and 0.015 M Na_2HPO_4, pH 7.4) at room temperature for 3×5 min. Before clearing, fresh refractive index matching solution (RIMS, 133% Histodenz, Sigma-Aldrich D2158) in 0.02 M PB was prepared and applied to the samples after careful removal of PB. Clearing was performed at 4°C on a shaking incubator for at least 24 h.

Histology

PFA fixed E12.5 embryos were dehydrated through an ethanol series in 30%, 50% and 2×70% ethanol for 15 min each, processed in a MICROM STP 120 processor (Microm 813150) and embedded in paraffin wax (Leica 3801320) using an EC 350-1 embedding station (Microm). Sections of 10 µm thickness were prepared using a rotary microtome (Microm, HM355S), transferred onto adhesion microscope slides (Menzel K5800AMNZ72) and dried overnight at 37°C. Eosin (Merck 109844) counterstaining was performed according to standard procedures and specimens were mounted in Enthellan (Sigma-Aldrich 107960). Sections were imaged using an AxioZoom V16 stereomicroscope (Zeiss).

Microscopy

Embryos were imaged using a Zeiss LSM880 laser scanning microscope with Airyscan detector or Zeiss Light sheet LS Z1 with appropriate filters for mCherry, Venus, DAPI, Alexa488 and Alexa647. For light-sheet microscopy, specimens were cleared and embedded in 1.5% low melting agarose (Sigma-Aldrich A9414)/PBS. Agarose columns containing the samples were inserted into the RIMS filled acquisition chamber and cleared for an additional 5 h to overnight depending on tissue volume. Post-acquisition processing was performed using ZEN Blue/Black (Zeiss) software or Arivis Vision 4D (Arivis).

In vitro differentiation of Noto^{mC} cells

In vitro generation of notochord cells was performed using a modification of a previously published protocol (Winzi et al., 2011). Embryonic stem cells were seeded on 6 cm plates and passaged two times until about 70% confluence. Cells were trypsinized and resuspended in 2 ml ES+LIF. Feeder cells were depleted from single cell suspensions by sequential plating on 0.1% gelatin (Sigma G1393)-coated six-well plates (Corning 3335) in 25 min, 20 min and 15 min intervals. After feeder freeing, cells were resuspended in 1 ml NotoDiff medium (Knock Out Knockout Dulbecco's Modified Eagle's Medium with 100 µM sodium pyruvate (Gibco 10829-018), 1×N-2 Supplement (Gibco 17502-048), 1×B-27 Supplement w/o Vitamin A (Gibco 12587-010), 1×MEM non-essential amino acids (Gibco 1140-35), 5 µg/ml penicillin/streptomycin (Lonza DE17-603E), 100 µM β-mercaptothanol (Gibco 21985-023), 200 µM Glutamine (Lonza BE17-605E), counted and seeded on 0.1% gelatin (Sigma Aldrich G1393)-coated Nunclon Delta Surface 12-well plates (Thermo Scientific 150628) at a density of 5000 cells per well and per ml medium. During the 7 day differentiation protocol, medium was refreshed every 24 h. Cells were cultured in NotoDiff containing 1 ng/ml activin A (R&D Systems 338-AC) for 72 h. Subsequently, NotoDiff medium containing 1 ng/ml activin A (R&D Systems 338-AC), 100 ng/ml FGF2 (Peprotech 100-18B), 50 ng/ml Noggin (Peprotech 250-38), 1 µM AGN (Santa Cruz 193109) and 0.5 µM Smoothened agonist (Merck 364590-63-6) was applied for another 96 h.

ChIP-Seq

For the identification of putative notochord enhancers, chromatin immunoprecipitation (ChIP) for T was performed using Noto-differentiated

cells at D7, following a previously published protocol (Koch et al., 2011). ChIP-Seq sequencing libraries were generated using the TrueSeq ChIP-Seq kit (Ilumina) following the manufacturer's instructions with minor modifications. After adapter ligation, 0.95× of AMPure XP beads (Beckman Coulter A63880) were used for a single purification and the DNA was eluted using 15 µl of resuspension buffer (RSB, Illumina). After the addition of 1 µl primer mix (25 mM each: Primer 1, 5′-AATGATACGGCGACCACCGA*G-3′; and Primer 2, 5′-CAAGCAGAAGACGGCATACGA*G-3′) and 15 µl 2× Kapa HiFi HotStart Ready Mix (Kapa Biosystems), amplification was performed for 45 s at 98°C, five cycles of [15 s at 98°C, 30 s at 63°C and 30 s at 72°C] and a final 1 min incubation at 72°C. The PCR products were purified using 0.95× of beads and eluted using 21 µl of RSB. Libraries were directly amplified for additional 13 cycles and purified using AMPure XP beads. The libraries were quantified using the Qubit DNA HS assay and the library size was validated using DNA HS bioanalyzer chips (Agilent 5067-4626).

Reads were mapped to chromosomes 1-19, X, Y and M of the mouse mm10 genome using bowtie version 1.1.2 (Langmead et al., 2009), providing the options '-y -m 1 -S -I 100 -X 500'. The mapping information of the paired-end reads was used to elongate each fragment to its original size using a custom pearl script, with the result stored as a BED file. Reads were then sorted and deduplicated such that only one fragment with the same starting and end position was retained. For visualization, wiggle files were generated with BEDTools version 2.23.0 (Quinlan and Hall, 2010), converted to bigwig format and analyzed in the Integrated Genome Browser (Freese et al., 2016).

Acknowledgements
We are grateful to the MPIMG transgenic unit and animal facility, especially Karol Macura, Judith Fiedler, Adrian Landsberger, Mirjam Peetz, Dijana Mićić and Christin Franke for performing the morula aggregation experiments and animal husbandry. We thank Sandra Währisch and Gaby Bläß for tissue culture support, Fabian Tobor for helping to establish the notochord differentiation protocol, Claudia Giesecke-Thiel and Uta Marchfelder from the MPIMG flow cytometry unit for FACS support, and all members of the MPIMG microscopy and sequencing core facilities for technical support.

Competing interests
The authors declare no competing or financial interests.

Author contributions
Conceptualization: B.G.H.; Methodology: L.W., J.V.V., F.K.; Software: F.K.; Validation: D.S., B.G.H.; Investigation: D.S., M.S.-W.; Resources: M.S.-W., L.W., F.K.; Data curation: F.K.; Writing - original draft: D.S., B.G.H.; Writing - review & editing: D.S., J.V.V., F.K., B.G.H.; Visualization: D.S.; Supervision: F.K., B.G.H.; Project administration: B.G.H.; Funding acquisition: B.G.H.

Funding
All funding was provided by the Max-Planck-Gesellschaft. J.V.V. was partially funded by an Alexander von Humboldt-Stiftung fellowship. Open access funding provided by the Max Planck Society. Deposited in PMC for immediate release.

Data availability
The sequencing data reported in this paper has been deposited in GEO under accession number GSE179665.

Peer review history
The peer review history is available online at https://journals.biologists.com/dev/article-lookup/doi/10.1242/dev.200059.

References
Ang, S.-L. and Rossant, J. (1994). *HNF*-3β is essential for node and notochord formation in mouse development. *Cell* **78**, 561-574. doi:10.1016/0092-8674(94)90522-3

Arnold, S. J., Stappert, J., Bauer, A., Kispert, A., Herrmann, B. G. and Kemler, R. (2000). Brachyury is a target gene of the Wnt/β-catenin signaling pathway. *Mech. Dev.* **91**, 249-258. doi:10.1016/S0925-4773(99)00309-3

Beddington, R. S. (1994). Induction of a second neural axis by the mouse node. *Development* **120**, 613-620. doi:10.1242/dev.120.3.613

Cambray, N. and Wilson, V. (2002). Axial progenitors with extensive potency are localised to the mouse chordoneural hinge. *Development* **129**, 4855-4866. doi:10.1242/dev.129.20.4855

Cambray, N. and Wilson, V. (2007). Two distinct sources for a population of maturing axial progenitors. *Development* **134**, 2829-2840. doi:10.1242/dev.02877

Chalamalasetty, R. B., Garriock, R. J., Dunty, W. C., Jr., Kennedy, M. W., Jailwala, P., Si, H. and Yamaguchi, T. P. (2014). Mesogenin 1 is a master regulator of paraxial presomitic mesoderm differentiation. *Development* **141**, 4285-4297. doi:10.1242/dev.110908

Chesley, P. (1935). Development of the short-tailed mutant in the house mouse. *J. Exp. Zool.* **70**, 429-459. doi:10.1002/jez.1400700306

Chiang, C., Litingtung, Y., Lee, E., Young, K. E., Corden, J. L., Westphal, H. and Beachy, P. A. (1996). Cyclopia and defective axial patterning in mice lacking Sonic hedgehog gene function. *Nature* **383**, 407-413. doi:10.1038/383407a0

Clements, D., Taylor, H. C., Herrmann, B. G. and Stott, D. (1996). Distinct regulatory control of the Brachyury gene in axial and non-axial mesoderm suggests separation of mesoderm lineages early in mouse gastrulation. *Mech. Dev.* **56**, 139-149. doi:10.1016/0925-4773(96)00520-5

Dobrovolskaia-Zavadskaia, N. (1927). Sur la mortification spontanee de la queuw chez la spuris nouveau et sur l'existence d'un caractere (facteur) hereditaire non viable. *Compr. Soc. Biol.* **97**, 114-119.

Eakin, G. S. and Hadjantonakis, A.-K. (2006). Production of chimeras by aggregation of embryonic stem cells with diploid or tetraploid mouse embryos. *Nat. Protoc.* **1**, 1145-1153. doi:10.1038/nprot.2006.173

Edri, S., Hayward, P., Jawaid, W. and Martinez Arias, A. (2019). Neuro-mesodermal progenitors (NMPs): a comparative study between pluripotent stem cells and embryo-derived populations. *Development* **146**, dev180190. doi:10.1242/dev.180190

Fernandes-Alnemri, T., Litwack, G. and Alnemri, E. S. (1994). CPP32, a novel human apoptotic protein with homology to Caenorhabditis elegans cell death protein Ced-3 and mammalian interleukin-1 beta-converting enzyme. *J. Biol. Chem.* **269**, 30761-30764. doi:10.1016/S0021-9258(18)47344-9

Freese, N. H., Norris, D. C. and Loraine, A. E. (2016). Integrated genome browser: visual analytics platform for genomics. *Bioinformatics* **32**, 2089-2095. doi:10.1093/bioinformatics/btw069

Garriock, R. J., Chalamalasetty, R. B., Kennedy, M. W., Canizales, L. C., Lewandoski, M. and Yamaguchi, T. P. (2015). Lineage tracing of neuromesodermal progenitors reveals novel Wnt-dependent roles in trunk progenitor cell maintenance and differentiation. *Development* **142**, 1628-1638. doi:10.1242/dev.111922

Gentsch, G. E., Owens, N. D. L., Martin, S. R., Piccinelli, P., Faial, T., Trotter, M. W. B., Gilchrist, M. J. and Smith, J. C. (2013). In vivo T-box transcription factor profiling reveals joint regulation of embryonic neuromesodermal bipotency. *Cell Rep.* **4**, 1185-1196. doi:10.1016/j.celrep.2013.08.012

George, S. H. L., Gertsenstein, M., Vintersten, K., Korets-Smith, E., Murphy, J., Stevens, M. E., Haigh, J. J. and Nagy, A. (2007). Developmental and adult phenotyping directly from mutant embryonic stem cells. *Proc. Natl. Acad. Sci. USA* **104**, 4455-4460. doi:10.1073/pnas.0609277104

Gluecksohn-Schoenheimer, S. (1944). The development of normal and homozygous brachy (T/T) mouse embryos in the extraembryonic coelom of the chick. *Proc. Natl. Acad. Sci. USA* **30**, 134-140. doi:10.1073/pnas.30.6.134

Gouti, M., Delile, J., Stamataki, D., Wymeersch, F. J., Huang, Y., Kleinjung, J., Kleinjung, J., Wilson, V. and Briscoe, J. (2017). A gene regulatory network balances neural and mesoderm specification during vertebrate trunk development. *Dev. Cell* **41**, 243-261.e7. doi:10.1016/j.devcel.2017.04.002

Henrique, D., Abranches, E., Verrier, L. and Storey, K. G. (2015). Neuromesodermal progenitors and the making of the spinal cord. *Development* **142**, 2864-2875. doi:10.1242/dev.119768

Herrmann, B. G., Labeit, S., Poustka, A., King, T. R. and Lehrach, H. (1990). Cloning of the T gene required in mesoderm formation in the mouse. *Nature* **343**, 617-622. doi:10.1038/343617a0

Hofmann, M., Schuster-Gossler, K., Watabe-Rudolph, M., Aulehla, A., Herrmann, B. G. and Gossler, A. (2004). WNT signaling, in synergy with T/TBX6, controls Notch signaling by regulating Dll1 expression in the presomitic mesoderm of mouse embryos. *Genes Dev.* **18**, 2712-2717. doi:10.1101/gad.1248604

Jurberg, A. D., Aires, R., Varela-Lasheras, I., Nóvoa, A. and Mallo, M. (2013). Switching axial progenitors from producing trunk to tail tissues in vertebrate embryos. *Dev. Cell* **25**, 451-462. doi:10.1016/j.devcel.2013.05.009

Kinder, S. J., Tsang, T. E., Wakamiya, M., Sasaki, H., Behringer, R. R., Nagy, A. and Tam, P. P. L. (2001). The organizer of the mouse gastrula is composed of a dynamic population of progenitor cells for the axial mesoderm. *Development* **128**, 3623-3634. doi:10.1242/dev.128.18.3623

Koch, F., Fenouil, R., Gut, M., Cauchy, P., Albert, T. K., Zacarias-Cabeza, J., Spicuglia, S., de la Chapelle, A. L., Heidemann, M., Hintermair, C. et al. (2011). Transcription initiation platforms and GTF recruitment at tissue-specific enhancers and promoters. *Nat. Struct. Mol. Biol.* **18**, 956-963. doi:10.1038/nsmb.2085

Koch, F., Scholze, M., Wittler, L., Schifferl, D., Sudheer, S., Grote, P., Timmermann, B., Macura, K. and Herrmann, B. G. (2017). Antagonistic

activities of Sox2 and brachyury control the fate choice of neuro-mesodermal progenitors. *Dev. Cell* **42**, 514-526.e7. doi:10.1016/j.devcel.2017.07.021

Langmead, B., Trapnell, C., Pop, M. and Salzberg, S. L. (2009). Ultrafast and memory-efficient alignment of short DNA sequences to the human genome. *Genome Biol.* **10**, R25. doi:10.1186/gb-2009-10-3-r25

Martin, B. L. and Kimelman, D. (2008). Regulation of canonical Wnt signaling by Brachyury is essential for posterior mesoderm formation. *Dev. Cell* **15**, 121-133. doi:10.1016/j.devcel.2008.04.013

Martin, B. L. and Kimelman, D. (2010). Brachyury establishes the embryonic mesodermal progenitor niche. *Genes Dev.* **24**, 2778-2783. doi:10.1101/gad.1962910

Martin, B. L. and Kimelman, D. (2012). Canonical Wnt signaling dynamically controls multiple stem cell fate decisions during vertebrate body formation. *Dev. Cell* **22**, 223-232. doi:10.1016/j.devcel.2011.11.001

Muyrers, J. P. P., Zhang, Y., Testa, G. and Stewart, A. F. (1999). Rapid modification of bacterial artificial chromosomes by ET-recombination. *Nucleic Acids Res.* **27**, 1555-1557. doi:10.1093/nar/27.6.1555

Pennimpede, T., Proske, J., König, A., Vidigal, J. A., Morkel, M., Bramsen, J. B., Herrmann, B. G. and Wittler, L. (2012). In vivo knockdown of Brachyury results in skeletal defects and urorectal malformations resembling caudal regression syndrome. *Dev. Biol.* **372**, 55-67. doi:10.1016/j.ydbio.2012.09.003

Perantoni, A. O., Timofeeva, O., Naillat, F., Richman, C., Pajni-Underwood, S., Wilson, C., Vainio, S., Dove, L. F. and Lewandoski, M. (2005). Inactivation of FGF8 in early mesoderm reveals an essential role in kidney development. *Development* **132**, 3859-3871. doi:10.1242/dev.01945

Porter, A. G. and Jänicke, R. U. (1999). Emerging roles of caspase-3 in apoptosis. *Cell Death Differ.* **6**, 99-104. doi:10.1038/sj.cdd.4400476

Quinlan, A. R. and Hall, I. M. (2010). BEDTools: a flexible suite of utilities for comparing genomic features. *Bioinformatics* **26**, 841-842. doi:10.1093/bioinformatics/btq033

Rennebeck, G. M., Lader, E., Chen, Q., Bohm, R. A., Cai, Z. S., Faust, C., Magnuson, T., Pease, L. R. and Artzt, K. (1995). Is there abrachyury the second? Analysis of a transgenic mutation involved in notochord maintenance in mice. *Dev. Biol.* **172**, 206-217. doi:10.1006/dbio.1995.0016

Stemple, D. L. (2005). Structure and function of the notochord: an essential organ for chordate development. *Development* **132**, 2503-2512. doi:10.1242/dev.01812

Stott, D., Kispert, L. A. and Herrmann, B. G. (1993). Rescue of the tail defect of Brachyury mice. *Genes Dev.* **7**, 197-203. doi:10.1101/gad.7.2.197

Teillet, M., Watanabe, Y., Jeffs, P., Duprez, D., Lapointe, F. and Le Douarin, N. M. (1998). Sonic hedgehog is required for survival of both myogenic and chondrogenic somitic lineages. *Development* **125**, 2019-2030. doi:10.1242/dev.125.11.2019

Tsakiridis, A. and Wilson, V. (2015). Assessing the bipotency of in vitro-derived neuromesodermal progenitors. *F1000Research* **4**, 100. doi:10.12688/f1000research.6345.1

Turner, D. A., Hayward, P. C., Baillie-Johnson, P., Rué, P., Broome, R., Faunes, F. and Martinez Arias, A. (2014). Wnt/β-catenin and FGF signalling direct the specification and maintenance of a neuromesodermal axial progenitor in ensembles of mouse embryonic stem cells. *Development* **141**, 4243-4253. doi:10.1242/dev.112979

Tzouanacou, E., Wegener, A., Wymeersch, F. J., Wilson, V. and Nicolas, J.-F. (2009). Redefining the progression of lineage segregations during mammalian embryogenesis by clonal analysis. *Dev. Cell* **17**, 365-376. doi:10.1016/j.devcel.2009.08.002

Ukita, K., Hirahara, S., Oshima, N., Imuta, Y., Yoshimoto, A., Jang, C.-W., Oginuma, M., Saga, Y., Behringer, R. R., Kondoh, H. et al. (2009). Wnt signaling maintains the notochord fate for progenitor cells and supports the posterior extension of the notochord. *Mech. Dev.* **126**, 791-803. doi:10.1016/j.mod.2009.08.003

Vidigal, J. A., Morkel, M., Wittler, L., Brouwer-Lehmitz, A., Grote, P., Macura, K. and Herrmann, B. G. (2010). An inducible RNA interference system for the functional dissection of mouse embryogenesis. *Nucleic Acids Res.* **38**, e122-e122. doi:10.1093/nar/gkq199

Weinstein, D. C., Ruiz i Altaba, A., Chen, W. S., Hoodless, P., Prezioso, V. R., Jessell, T. M. and Darnell, J. E. (1994). The winged-helix transcription factor HNF-3β is required for notochord development in the mouse embryo. *Cell* **78**, 575-588. doi:10.1016/0092-8674(94)90523-1

Wilkinson, D. G., Bhatt, S. and Herrmann, B. G. (1990). Expression pattern of the mouse T gene and its role in mesoderm formation. *Nature* **343**, 657-659. doi:10.1038/343657a0

Wilson, V., Olivera-Martinez, I. and Storey, K. G. (2009). Stem cells, signals and vertebrate body axis extension. *Development* **136**, 1591-1604. doi:10.1242/dev.021246

Winzi, M. K., Hyttel, P., Dale, J. K. and Serup, P. (2011). Isolation and characterization of node/notochord-like cells from mouse embryonic stem cells. *Stem Cells Dev.* **20**, 1817-1827. doi:10.1089/scd.2011.0042

Wittler, L., Shin, E.-h., Grote, P., Kispert, A., Beckers, A., Gossler, A., Werber, M. and Herrmann, B. G. (2007). Expression of Msgn1 in the presomitic mesoderm is controlled by synergism of WNT signalling and Tbx6. *EMBO Rep.* **8**, 784-789. doi:10.1038/sj.embor.7401030

Wymeersch, F. J., Huang, Y., Blin, G., Cambray, N., Wilkie, R., Wong, F. C. K. and Wilson, V. (2016). Position-dependent plasticity of distinct progenitor types in the primitive streak. *eLife* **5**, e10042. doi:10.7554/eLife.10042

Wymeersch, F. J., Skylaki, S., Huang, Y., Watson, J. A., Economou, C., Marek-Johnston, C., Tomlinson, S. R. and Wilson, V. (2019). Transcriptionally dynamic progenitor populations organised around a stable niche drive axial patterning. *Development* **146**, dev168161. doi:10.1242/dev.168161

Wymeersch, F. J., Wilson, V. and Tsakiridis, A. (2021). Understanding axial progenitor biology in vivo and in vitro. *Development* **148**, dev180612. doi:10.1242/dev.180612

Yamaguchi, T. P., Takada, S., Yoshikawa, Y., Wu, N. and McMahon, A. P. (1999). T (Brachyury) is a direct target of Wnt3a during paraxial mesoderm specification. *Genes Dev.* **13**, 3185-3190. doi:10.1101/gad.13.24.3185

Yamanaka, Y., Tamplin, O. J., Beckers, A., Gossler, A. and Rossant, J. (2007). Live imaging and genetic analysis of mouse notochord formation reveals regional morphogenetic mechanisms. *Dev. Cell* **13**, 884-896. doi:10.1016/j.devcel.2007.10.016

Zhu, J., Kwan, K. M. and Mackem, S. (2016). Putative oncogene Brachyury (T) is essential to specify cell fate but dispensable for notochord progenitor proliferation and EMT. *Proc. Natl. Acad. Sci. USA* **113**, 3820-3825. doi:10.1073/pnas.1601252113

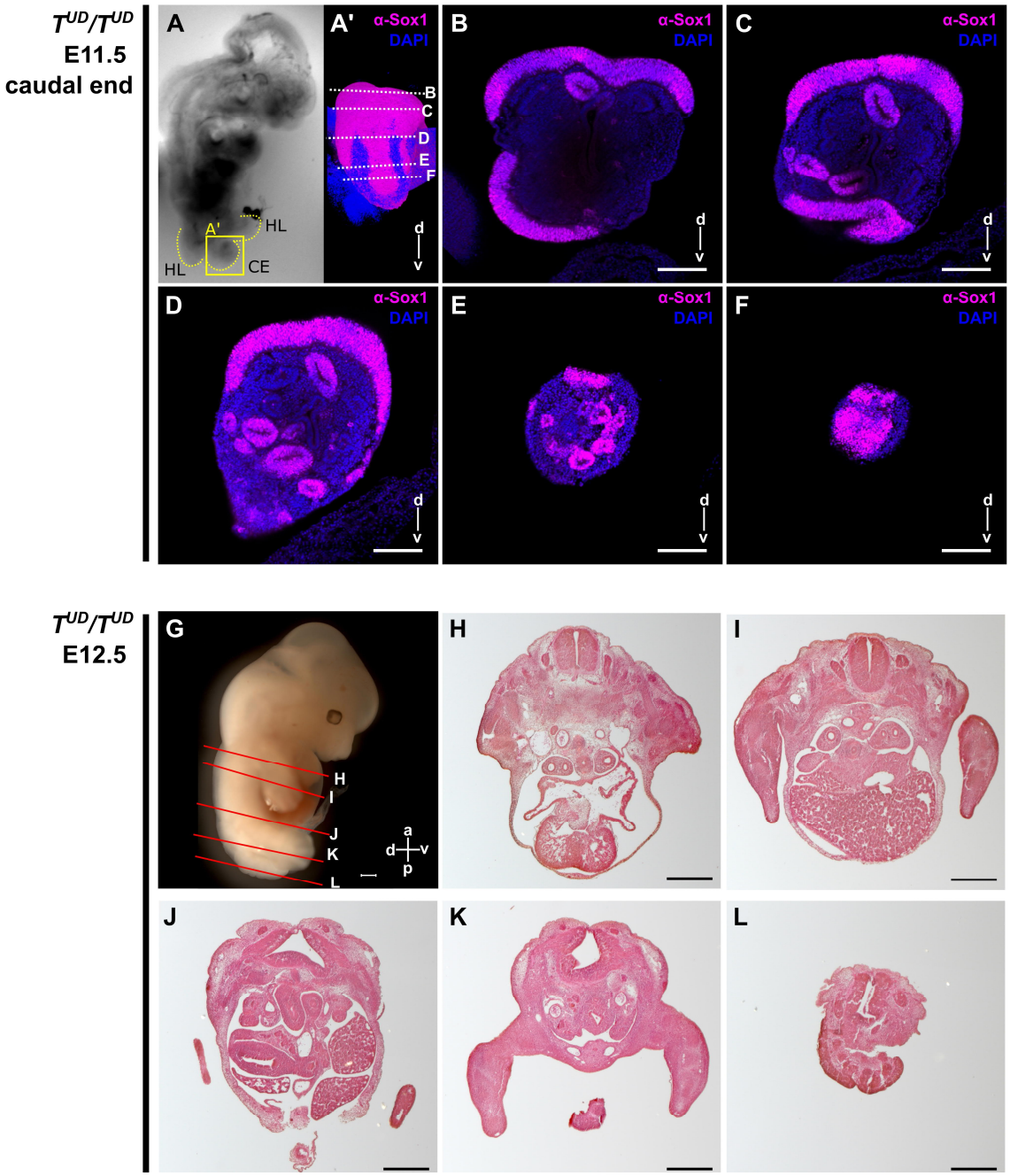

Fig. S1. Excess neural tissue is formed in the caudal end of T^{UD}/T^{UD} mutants

(A) Bright field image of a cleared T^{UD}/T^{UD} mutant embryo. HL = Hind limb. CE = Caudal End. **(A')** Maximum intensity projection of Light sheet micrographs from the caudal end region indicated by the yellow box in (A). White lines indicate the positions of optical transversal sections shown in (B-F). **(B-F)** Caudal tissue with immunofluorescence for Sox1 marking neural tissue. Transversal optical sections acquired by Light Sheet microscopy. Scale bar = 200 µm **(G)**: Lateral view of a E12.5 T^{UD}/T^{UD} mutant embryo. Red lines indicate the section planes. **(H-L)**: Histological transversal sections demonstrating massive morphological disorganization, in particular of the spinal cord (J-L). Scale bar = 500 µm. a = anterior. p = posterior. d = dorsal. v = ventral.

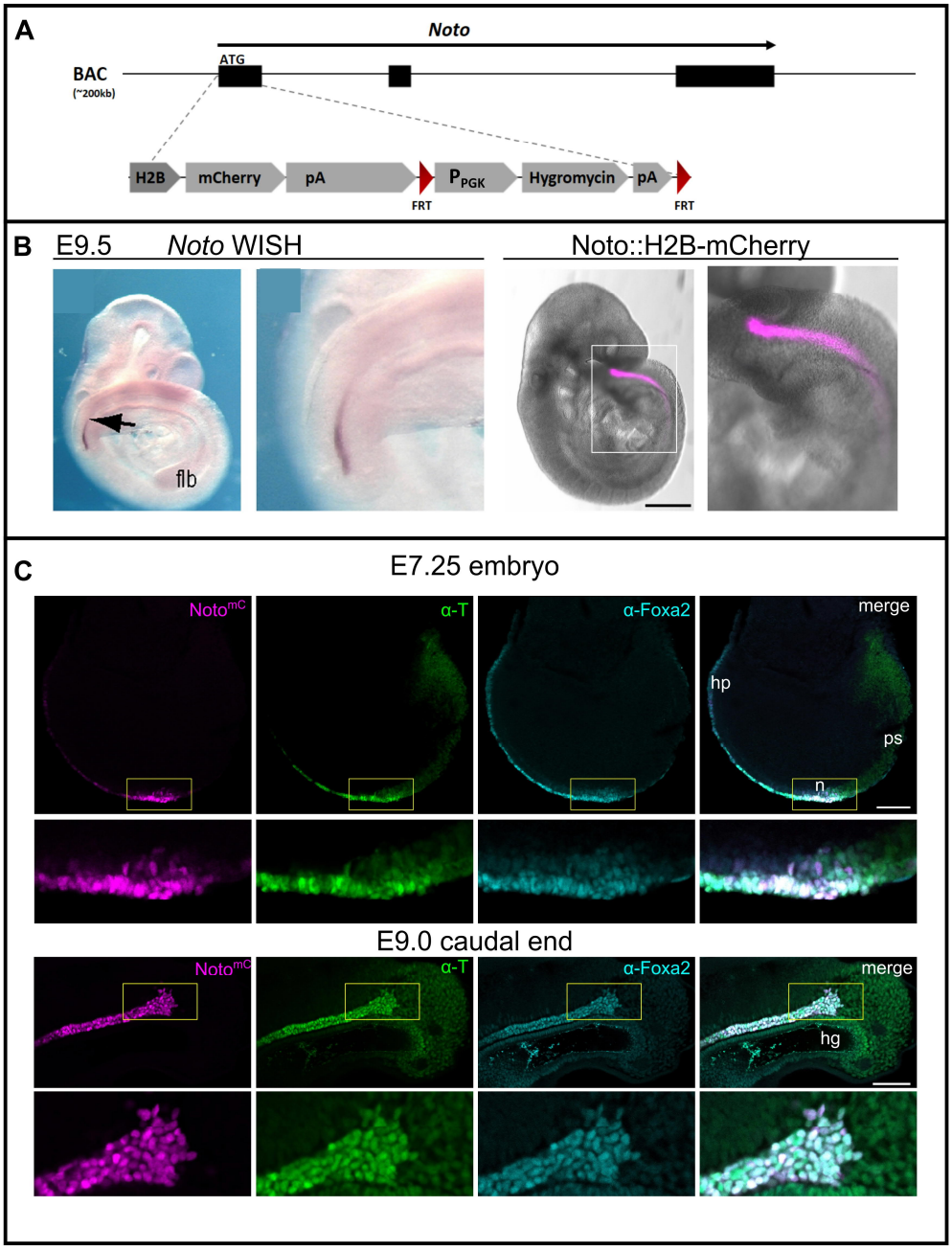

Fig. S2. Establishment of a Noto reporter mESC line

(A) Schematic representation of the *Noto::H2B-mCherry* reporter BAC. **(B)** Left: *Noto* whole mount *in situ* hybridization adapted from Pennimpede et al, 2012. flb = forelimb bud. Right: Noto^{mC} reporter fluorescence in a E9.5 embryo acquired by stereomicroscopy. Scale bar = 500 µm. **(C)** Confocal fluorescence microscopy of a E7.25 early headfold stage embryo and a E9.0 caudal end with Noto^{mC} reporter expression (magenta) and immunofluorescence for T (green) and Foxa2 (cyan). At E7.25, Noto^{mC} can be detected in the ventral node, head process notochord, crown cells and cells in the midline of the epiblast. At E9.0. Noto^{mC} marks the posterior end of the notochord. Scale bar = 100 µm. hp = head process. n = node. ps = primitive streak. hg = hindgut.

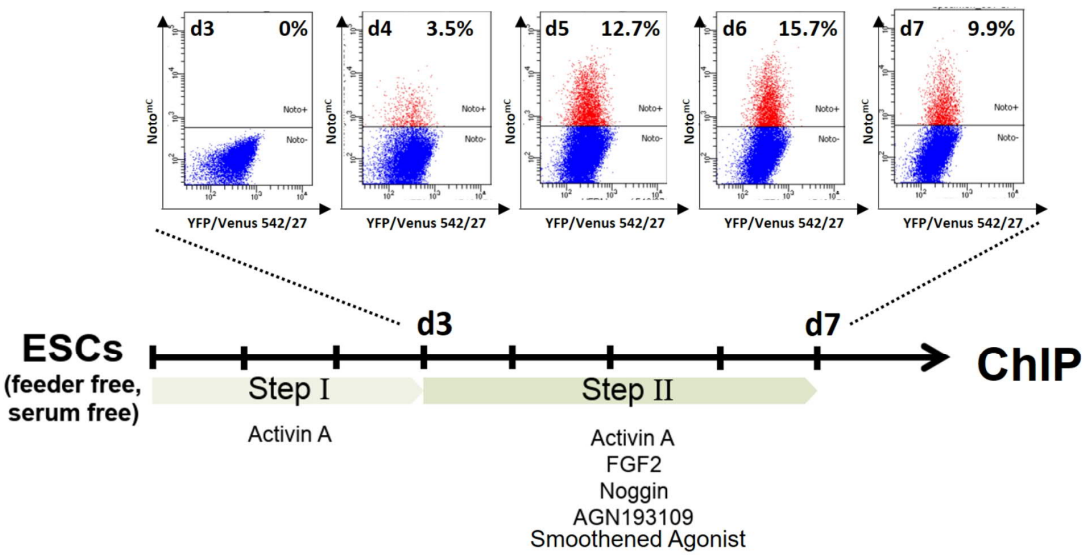

Fig. S3. Schematic representation of the notochord differentiation procedure

FACS plots show the proportion of Noto^{mC} expressing cells after application of step II medium at d3 in an exemplary experiment. For transcription factor ChIP-Seq, bulk cells were harvested between d6 and d7 of the procedure.

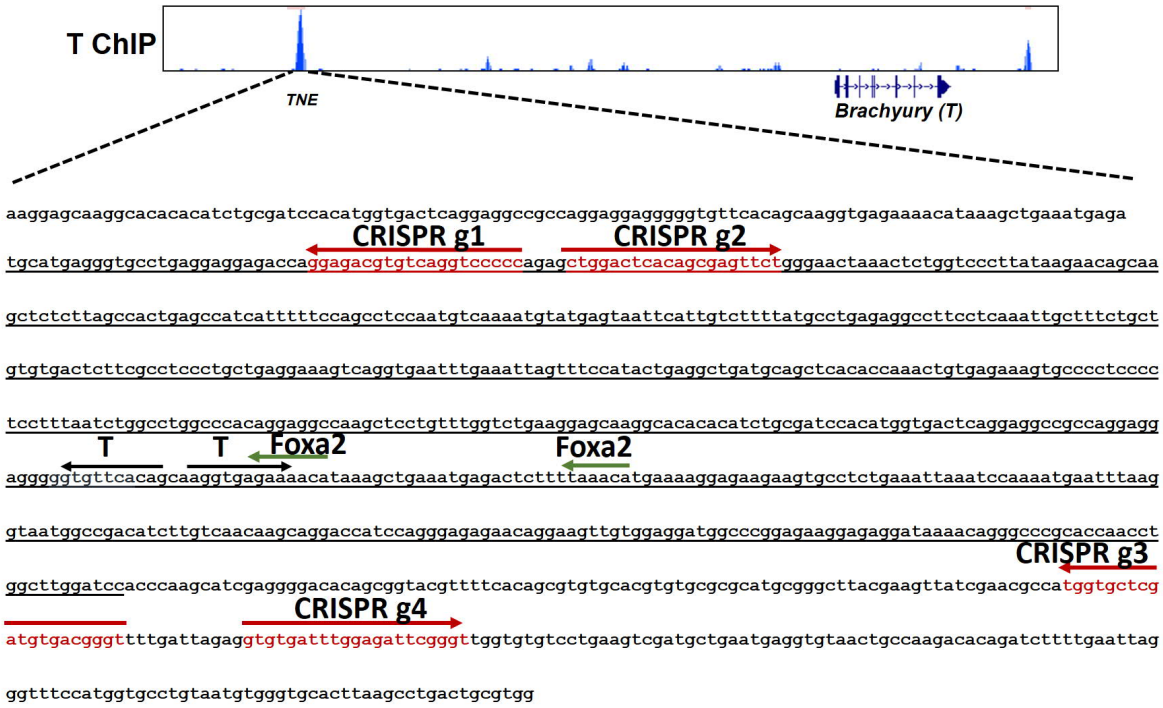

aaggagcaaggcacacacatctgcgatccacatggtgactcaggaggccgccaggaggaggggtgttcacagcaaggtgagaaaacataaagctgaaatgaga

tgcatgagggtgcctgaggaggagaccaggagacgtgtcaggtccccc agagctggactcacagcgagttct gggaactaaactctggtcccttataagaacagcaa

gctctcttagccactgagccatcatttttccagcctccaatgtcaaaatgtatgagtaattcattgtcttttatgcctgagaggccttcctcaaattgctttctgct

gtgtgactcttcgcctccctgctgaggaaagtcaggtgaatttgaaattagtttccatactgaggctgatgcagctcacaccaaactgtgagaaagtgcccctcccc

tcctttaatctggcctggcccacaggaggccaagctcctgtttggtctgaaggagcaaggcacacacatctgcgatccacatggtgactcaggaggccgccaggagg

aggggg tgttcacagcaaggtgagaaaacataaagctgaaatgagactcttttaaacatgaaaaggagaagaagtgcctctgaaattaaatccaaaatgaatttaag

gtaatggccgacatcttgtcaacaagcaggaccatccagggagagaacaggaagttgtggaggatggcccggagaaggagaggataaaacagggcccgcaccaacct

ggcttggatcc acccaagcatcgaggggacacagcggtacgttttcacagcgtgtgcacgtgtgcgcgcatgcgggcttacgaagttatcgaacgcca tggtgctcg

atgtgacgggt ttgattagag gtgtgatttggagattcgggt tggtgtgtcctgaagtcgatgctgaatgaggtgtaactgccaagacacagatcttttgaattag

ggtttccatggtgcctgtaatgtgggtgcacttaagcctgactgcgtgg

Fig. S4. *TNE* sequence

The sequence of the fragment tested in enhancer activity assays is underlined. Red letters and arrows indicate the guide RNA sequences used for CRISPR/Cas9 mediated deletions. Core binding motifs for T (black, palindromic consensus binding site) and Foxa2 (green) are highlighted. The ChIP-Seq track shows T binding sites in Noto^{diff} cells (this study).

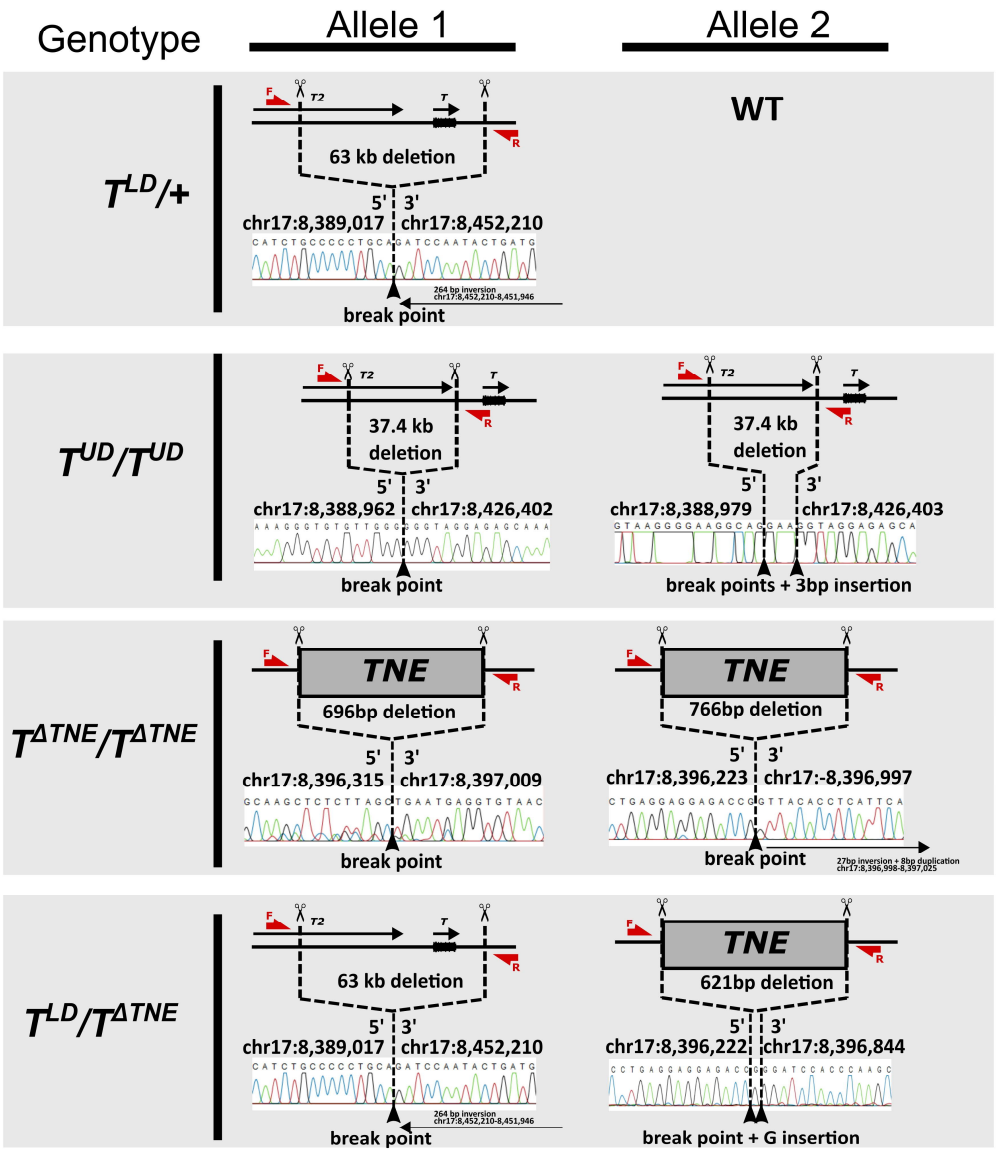

Fig. S5. Genotyping of Deletions

Red arrows indicate the position of the forward (F) and reverse (R) primers used for genotyping by PCR, not to scale. Scissors icons indicate the approximate positions of gRNA target sites. The dotted lines converging at the break point(s) mark the CRISPR/Cas9 mediated deletions. The coordinates (mm10) of the bordering 5' and 3' edges of the respective deletions are specified next to the break point(s). Sanger sequencing tracks of enhancer mutant PCR fragment or subcloned PCR fragments in case of double deletions show the region flanking the deletions. For each genotype at least two clones were generated and checked for phenotypic identity.

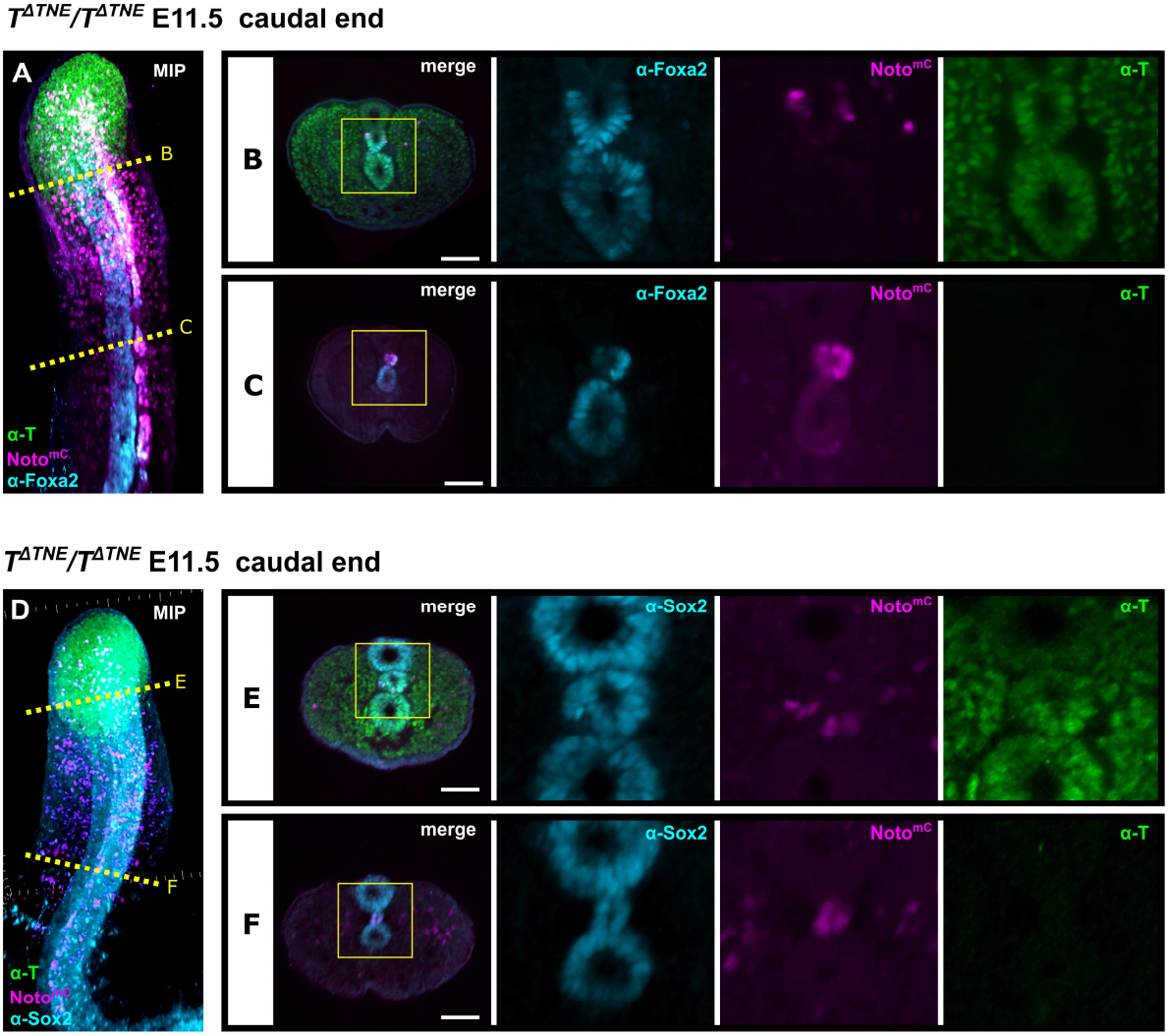

Fig. S6. Notochord progenitor cells in $T^{\Delta TNE}/T^{\Delta TNE}$ tailbuds are mal-specified and contribute to paraxial mesoderm and ectopic endodermal or ventral neural tube-like structures

(A) Maximum intensity projection of Light sheet micrographs of E11.5 tailbud with immunofluorescence for Foxa2 (cyan) and T (green). Yellow lines indicate the positions of optical sections shown in (B,C). **(B-C)** Transversal optical sections acquired by Light Sheet microscopy. Scale bar = 100 µm **(D)** Maximum intensity projection of Light Sheet micrographs of E11.5 tailbud with immunofluorescence for Sox2 (cyan) and T (green). Yellow lines indicate the positions of optical sections shown in (B,C). **(E-F)** Transversal optical sections acquired by Light Sheet microscopy. Scale bar = 100 µm. Noto^{mC} cells mostly contribute to paraxial mesoderm. An ectopic tubular midline structure formed between the neural tube and the gut expresses T, Sox2 and Foxa2 in the tailbud, but only Sox2 and Foxa2 anterior to the tailbud, indicating that it does not have notochordal identity. The presence of Noto^{mC} cells, however, points to its (at least partial) derivation from mal-specified notochord progenitor cells. The expression of Sox2 and Foxa2 suggests that it has acquired either endodermal or ventral neural tube-like identity. Ectopic neural tube-like structures have previously been described in the posterior trunk of Shh-Cre;T-shRNA T-knockdown embryos (Zhu et al. 2016).

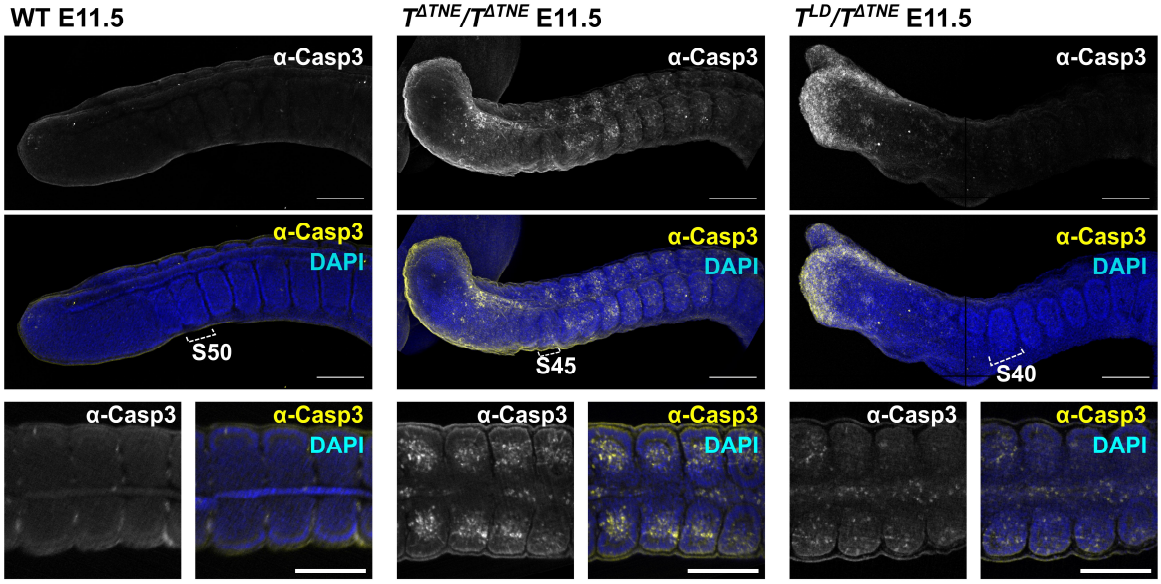

Fig. S7. Mutant tails lacking the notochord undergo apoptosis

Top: Maximum intensity projections of confocal stacks showing wild type (WT) and mutant tails. Extensive Caspase 3 (Casp3) immunofluorescence indicate massive induction of programmed cell death (reviewed in Porter and Jänicke, 1999) in mutant tails compared to wild type. The number of the last formed somite (S) is indicated. Casp3 signal shown as single channel and overlap with DAPI nuclear staining. Bottom: Coronal optical sections acquired by Light sheet microscopy showing strong Casp3 expression in somites and midline cells. Scale bar = 500 µm.

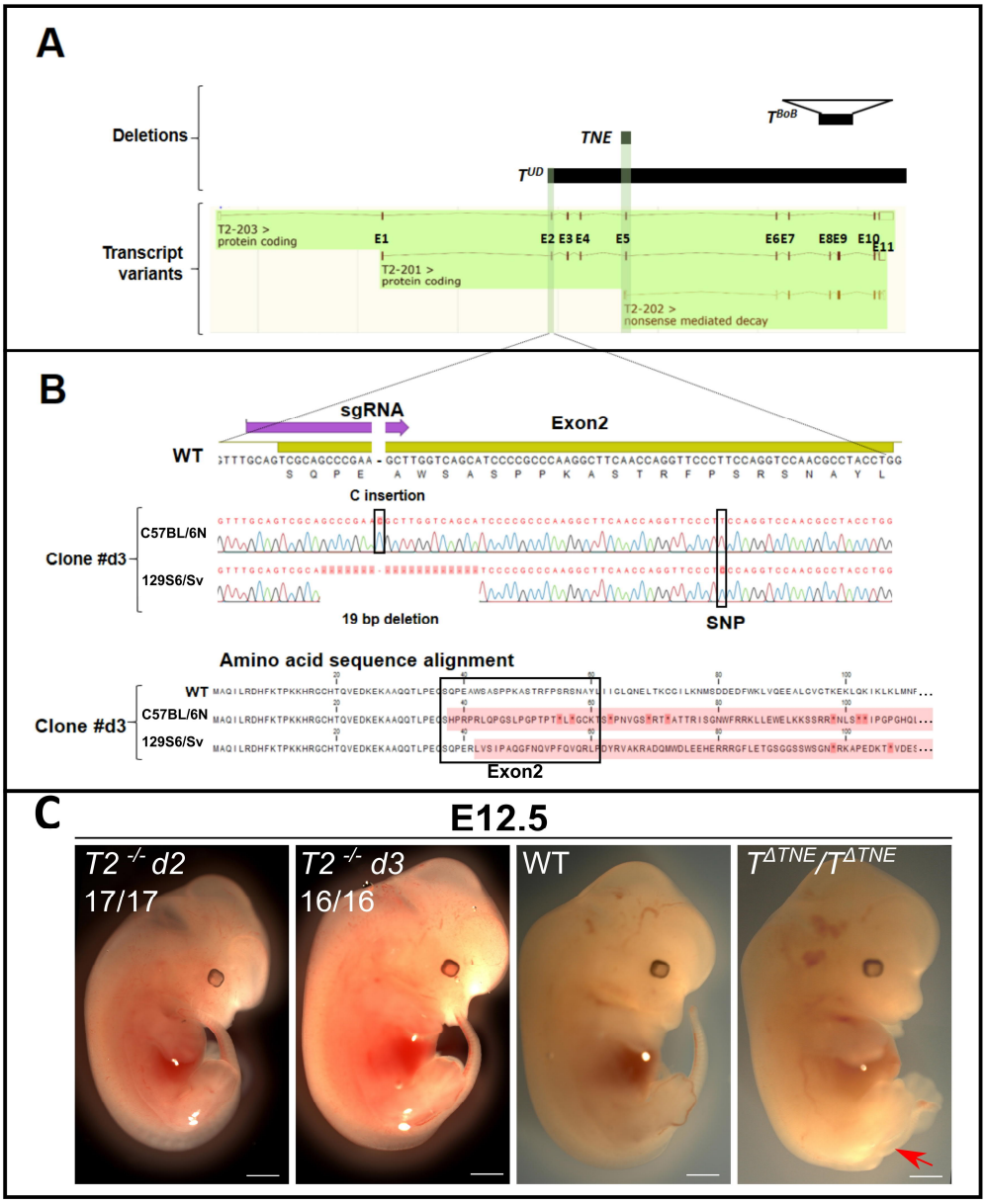

Fig. S8. Disruption of the T2 ORF does not induce a tail phenotype

(A) *T2* transcript variants annotated in the ensemble database. Location: Chromosome 17: 8,355,992- 8,423,513 forward strand (mm10). Top: Mutant genotypes covering exons of the transcript. **(B)** Knock-out strategy using a single CRISPR guide RNA to introduce indels in exon 2. Representative genotyping of one clone. Top: Sanger sequencing of subcloned PCR fragments. Because a hybrid cell line is used, the C57BL/6N and 129S6/Sv alleles were discriminated via a short nucleotide polymorphism. Bottom: Amino acid sequence alignment. Frameshift sequence highlighted in red, stop codons indicated by red asterisks. **(C)** E12.5 Embryos generated via tetraploid aggregation. *T2* -/- does not recapitulate the axial truncation phenotype of $T^{\Delta TNE}/T^{\Delta TNE}$ pointed out by the red arrow. Number of analyzed embryos with the same morphology indicated for *T2* $^{-/-}$ two independent clones (d2 and d3). Scale bar = 1 mm.

Table S1. List of oligonucleotides used for cloning and PCR

Name	5'-3' Sequence	Purpose
T-dup-u_F1	CCTTTCCCCCTTGATCAC	T^{CD} CRISPR genotyping PCR
Noto_rec_H2B-mCherry_fw	CTCCCATTGAGCTCCTTGCACAGCCTGGGAGGTCCCCTCAGGGTCGCGCAATGCCAGAGCCAGCGAAGTC	BAC reporter recombineering PCR
Noto_rec_H2B-mCherry_rv	GGGCGCAGGCTCCCGGGCTGGACCTGAGTGCCTGAGGGAGCAGGGCTGGATTCCCAGTCACGACGTTGTA	BAC reporter recombineering PCR
Noto_PCR_fw	GGCCTCAATCAGCGATGATTAAG	BAC reporter recombineering PCR
Noto_PCR_rv	CTGGACCTGAGTGCCTGAG	BAC reporter recombineering PCR
PciI-Kozak-Venus_F	TTTTTACATGTCCGCCACCATGGTGAGCAAGGGCGAG	Enhancer reporter cloning
PciI-rbpA_R	TTTTTACATGTACGCGTGCAGTCGAGTTCATAAGAGAAGAGGGACAGCTATGACTGGGAGTAGTCAGGAGAGGAGGAAAAATCTGGCTAGTAAAAGATGTAAGGAAAATTTTAGGGATGT	Enhancer reporter cloning
Seq_U6_F	ACTATCATATGCTTACCGTAAC	Sequencing of gRNA vectors
T2_201_E2_g1_top	CACCGTGCAGTCGCAGCCCGAAGCT	T2 Indel CRISPR cloning
T2_201_E2_g1_bot	AAACAGCTTCGGGCTGCGACTGCAC	T2 Indel CRISPR cloning
T-ds_top	CACCGATCAGTATTGGATCCTCGTT	T^{CD} T CRISPR cloning
T-ds_bot	AAACAACGAGGATCCAATACTGATC	T^{CD} CRISPR cloning
T2_us_C1_top	CACCGATGCACGCTCTTAATCTCGG	T^{CD} CRISPR cloning
T2_us_C1_bot	AAACCCGAGATTAAGAGCGTGCATC	T^{CD} T CRISPR cloning
T_ds_R1	ATGAGAGTGCCTGAGGAG	T^{CD} T CRISPR genotyping PCR
T2_us_F	TATTGGGATGCTGTGCTC	T^{CD} T CRISPR genotyping PCR
T-45.5kb_top	CACCGGCTTCCAACTCCAAGGTAA	T^{UD} CRISPR cloning
T-45.5kb_bot	AAACTTACCTTGGAGTTGGAAGCC	T^{UD} CRISPR cloning
T-8kb8000_top	CACCGCAGCGTAGAGATAGCGGCT	T^{UD} CRISPR cloning
T-8kb000_bot	AAACAGCCGCTATCTCTACGCTGC	T^{UD} CRISPR cloning
T-8kb000_R	GTCTGTCCCTGAGATGATG	T^{UD} CRISPR genotyping PCR
T-45.5kb_F	GTGGCCAGCAAAGGGTGT	T^{UD} CRISPR genotyping PCR

TNE_sg1_top	CACCGGGGGACCTGACACGTCTCC	$T^{\Delta TNE}$ CRISPR cloning
TNE_sg1_bot	AAACGGAGACGTGTCAGGTCCCCC	$T^{\Delta TNE}$ CRISPR cloning
TNE_sg2_top	CACCGCTGGACTCACAGCGAGTTCT	$T^{\Delta TNE}$ CRISPR cloning
TNE_sg2_bot	AAACAGAACTCGCTGTGAGTCCAGC	$T^{\Delta TNE}$ CRISPR cloning
TNE_sg3_top	CACCGACCCGTCACATCGAGCACCA	$T^{\Delta TNE}$ CRISPR cloning
TNE_sg3_bot	AAACTGGTGCTCGATGTGACGGGTC	$T^{\Delta TNE}$ CRISPR cloning
TNE_sg4_top	CACCGTGTGATTTGGAGATTCGGGT	$T^{\Delta TNE}$ CRISPR cloning
TNE_sg4_bot	AAACACCCGAATCTCCAAATCACAC	$T^{\Delta TNE}$ CRISPR cloning

Table S2. Antibodies used for Immunofluorescence and ChIP

Description	Catalog number	Company	Host Organism	Concentration	Application
α-T	#81694	Cell Signaling Technology	Rabbit	1:250 in PBSTB	IF
α-Sox2	AF2018	R&D	Goat	1:250 in PBSTB	IF
α-Foxa2	sc-6554	Santa Cruz	Goat	1:250 in PBSTB	IF
α-Sox1	AF3369	R&D	Goat	Rabbit	IF
α-Olig2	AF2418	R&D	Goat	Rabbit	IF
α-Nkx2.2	ab191077	Abcam	Rabbit	Rabbit	IF
α-Caspase-3	9662S	Cell signaling Technology	Rabbit	1:250 in PBSTB	IF
Alexa Fluor 488 α-Rabbit	ab150073	Abcam	Donkey	1:250 in PBSTB	IF
Alexa Fluor 647 α-Goat	ab150135	Abcam	Donkey	1:250 in PBSTB	IF
α-T	AF2085	R&D	Goat	2.5µg	ChIP